Forecasting the ambient solar wind with numerical models. II. An adaptive prediction system for specifying solar wind speed near the Sun

Article

Accepted Version

Reiss, M. A., MacNeice, P. J., Muglach, K., Arge, C. N., Möstl, C., Riley, P., Hinterreiter, J., Bailey, R. L., Weiss, A. J., Owens, M. J. ORCID: https://orcid.org/0000-0003-2061-2453, Amerstorfer, T. and Amerstorfer, U. (2020) Forecasting the ambient solar wind with numerical models. II. An adaptive prediction system for specifying solar wind speed near the Sun. The Astrophysical Journal, 891 (2). 165. ISSN 1538-4357 doi: 10.3847/1538-4357/ab78a0 Available at https://centaur.reading.ac.uk/90943/

Draft version October 31, 2019
Typeset using LaTeX **preprint** style in AASTeX62

Forecasting the Ambient Solar Wind with Numerical Models. II. An Adaptive Prediction System for Specifying Solar Wind Speed Near the Sun

Martin A. Reiss,[1,2] Peter J. MacNeice,[1] Karin Muglach,[1,3] Charles N. Arge,[1] Christian Möstl,[2] Pete Riley,[4] Jürgen Hinterreiter,[2] Rachel L. Bailey,[2] Andreas J. Weiss,[2] Mathew J. Owens,[5] Ute Amerstorfer,[2] and Tanja Amerstorfer[2]

[1]*Heliophysics Science Division, NASA Goddard Space Flight Center, Greenbelt, MD 20771, USA*
[2]*Space Research Institute, Austrian Academy of Sciences, A-8042 Graz, Austria*
[3]*Catholic University of America, Washington, DC 20064, USA*
[4]*Predictive Science Inc., San Diego, CA 92121, USA*
[5]*Space and Atmospheric Electricity Group, Department of Meteorology, University of Reading, Reading, UK*

Abstract

The ambient solar wind flows and fields influence the complex propagation dynamics of coronal mass ejections in the interplanetary medium and play an **essential** role in driving Earth's space weather environment. A **critical** scientific goal in the space weather research and prediction community is to develop, implement and optimize numerical models for specifying the large-scale properties of solar wind conditions at the inner boundary of the heliospheric model domain. Here we present an adaptive prediction system that fuses information from in situ measurements of the solar wind into numerical models to better match the global solar wind model solutions near the Sun with prevailing physical conditions in the vicinity of Earth. In this way, we attempt to advance the predictive capabilities of well-established solar wind models for specifying solar wind speed, including the Wang-Sheeley (WS) model, Distance from the Coronal Hole Boundary (DCHB) model, and the Wang-Sheeley-Arge (WSA) model. **In particular, we use the Heliospheric Upwind eXtrapolation (HUX) model for mapping the solar wind solutions from the near-Sun environment to the vicinity of Earth. We present the newly developed Tunable HUX (THUX) model to solve the viscous form of the underlying Burgers equation.** We perform a statistical analysis of the resulting solar wind predictions for the time 2006–2015. We find that the proposed prediction scheme improves all the investigated coronal/heliospheric model combinations and produces better estimates of the solar wind state at Earth than our reference baseline model. **As an example, we apply the prediction scheme to the WSA/THUX model and find that the root mean**

Corresponding author: Martin A. Reiss
martin.reiss@oeaw.ac.at

square error reduces from 111.0 $\mathrm{km\,s^{-1}}$ **to 93.6** $\mathrm{km\,s^{-1}}$**, and that the Pearson correlation coefficient increases from 0.43 to 0.50.** We discuss why this is the case, and conclude that our findings have important implications for future practice in applied space weather research and prediction.

Keywords: Sun – ambient solar wind flow – solar-terrestrial relations

1. INTRODUCTION

The evolving ambient solar wind flow and the magnetic field embedded within it are driven by the Sun's magnetic field. **Thus, studying the magnetic field configuration in the solar atmosphere is of crucial importance for improving the understanding and ultimately the prediction of space weather from Sun to Earth. The magnetic configuration of open magnetic field lines, along which solar wind flows are accelerated to supersonic speeds is especially important for predicting key properties in the interplanetary medium alongside the solar wind bulk speed, magnetic field strength, and field orientation.** A considerable amount of literature has been published on reconstructing the global coronal magnetic field from photospheric magnetic field measurements due to the long-standing difficulty of mapping the magnetic field in the solar corona. The most popular techniques of this type are potential field source surface (PFSS; Altschuler and Newkirk 1969; Schatten et al. 1969), nonlinear force-free field (NLFF; see, for example, Schrijver et al. 2006), and magnetohydrodynamic (MHD; Riley et al. 2011) models, as recently reviewed by Mackay and Yeates (2012).

To seamlessly simulate the dynamics of the evolving ambient solar wind from the Sun to Earth, it is important to treat the photosphere, corona, and inner heliosphere as a coupled system. Therefore, operational systems for predicting the state in the evolving ambient solar wind rely **on the coupling of magnetic models of the corona** with models of the inner heliosphere (Riley et al. 2001; Lee et al. 2008). The coupled coronal-heliospheric modelling system spans the range from 1 solar radii (R_0) to 1 au, where the coronal model domain spans the range from 1 R_0 to 2.5 R_0 (PFSS) or 30 R_0 (MHD), and the heliospheric domain spans the range from 5–30 R_0 to 1 au using the global solar wind model solution from the magnetic model of the corona as an inner boundary condition. Currently, the most commonly used three-dimensional numerical MHD codes to derive stationary solutions for the ambient solar wind in the heliosphere are the Magnetohydrodynamics Algorithm outside a Sphere (MAS; Linker et al. 1999; Mikić et al. 1999), Enlil (Odstrcil 2003), the Space Weather Modeling Framework (SWMF; Tóth et al. 2005), and the recently developed European Heliospheric Forecasting Information Asset (EUHFORIA; Pomoell and Poedts 2018). The three-dimensional MHD model solutions are characterized by closed magnetic field lines confining the solar wind plasma and open field lines along which solar wind flows accelerate to supersonic speed and propagate into the heliosphere.

Since the major discovery by Wang and Sheeley (1990) of an empirical relationship between **the configuration** of open magnetic field lines and the solar wind state measured in the vicinity of Earth, a key scientific goal in the space weather research and prediction community is to develop and optimize empirical techniques for specifying the large-scale properties of the solar wind solution at the inner boundary of the heliospheric model domain (e.g., Arge and Pizzo 2000; Riley et al. 2001; Arge et al. 2004). **As the spatial and temporal structure in the wind flow** is determined by the

dynamic pressure term in the momentum equation, the solar wind bulk speed at the inner boundary dominates the propagation dynamics of the evolving ambient solar wind flow in the interplanetary medium (Riley et al. 2015). **Empirical techniques for specifying solar wind speed near the Sun are thus critical in providing input to solar wind models such as the Wang-Sheeley (WS; Wang and Sheeley 1990), Distance from the Coronal Hole Boundary (Riley et al. 2001, DCHB;), and Wang-Sheeley-Arge model (WSA; Arge et al. 2003). These empirical formulae either rely on the amount by which a magnetic flux tube expands between the solar surface and a given reference height in the corona (WS), the minimum angular distance of an open magnetic field footpoint from a coronal hole boundary (DCHB), or a combination of the two (WSA).**

Although the relative importance of the areal expansion factor and the minimum angular distance for specifying the characteristics of the magnetic field configuration in the solar corona is still under **debate** (see, Riley et al. 2015), the WSA model has become one of the workhorse models in the space weather community (e.g., Sheeley 2017). The coupled WSA/Enlil model is now routinely in use by the Space Weather Prediction Center (NOAA), and the Met Office Space Weather Operations Centre (MOSWOC) for operational space weather predictions of the solar wind state in the interplanetary medium and the arrival of coronal mass ejections at Earth. **Over the last decade, the WSA/Enlil model has been one of the most frequently used ambient solar wind models for studying the consequences of evolving space weather in the heliosphere.** Examples include the prediction of high-speed solar wind streams (Owens et al. 2005; MacNeice 2009a; Reiss et al. 2016), the prediction of arrival time and speed of coronal mass ejections (Taktakishvili et al. 2009; Wold et al. 2018; Riley et al. 2018; Verbeke et al. 2019), the study of the sensitivity of CME events to model parameter settings (Taktakishvili et al. 2010; Cash et al. 2015), the propagation of coronal mass ejections in the evolving ambient solar wind (Mays et al. 2015; Scolini et al. 2019), the prediction of solar energetic particles (MacNeice et al. 2011; Luhmann et al. 2017; Wijsen, N. et al. 2019), **the understanding of how** the evolving ambient solar wind flow interacts with planetary magnetospheres (Dewey et al. 2015), or the study of Forbush decreases in the flux of galactic cosmic rays (Winslow et al. 2018).

A considerable amount of literature has been published on validating ambient solar wind models such as the coupled WSA/Enlil model with in situ measurements at Earth (see, for instance, Owens et al. 2008; Jian et al. 2011; Owens et al. 2013; Devos et al. 2014). **These studies show that the predictive abilities of operational solar wind models are, if at all, only slightly better than a baseline model of recurrence assuming that conditions in the solar wind will persist after each synodic rotation of the Sun (e.g., Riley et al. 2015).** Advances in predicting the solar wind state in interplanetary **space** thus are of key importance for driving innovation in applied space weather research and prediction (see, Schrijver et al. 2015; Opgenoorth et al. 2019). **Here we present an adaptive model system that aims to improve the predictive capabilities of models of the evolving ambient solar wind by optimizing the model settings.** To this end, we propose an adaptive predictive system that fuses information from in situ measurements of the solar wind **from the previous Carrington Rotation (CR)** into numerical models to align the global solar wind model solutions near the Sun with prevailing physical conditions in the near-Earth space.

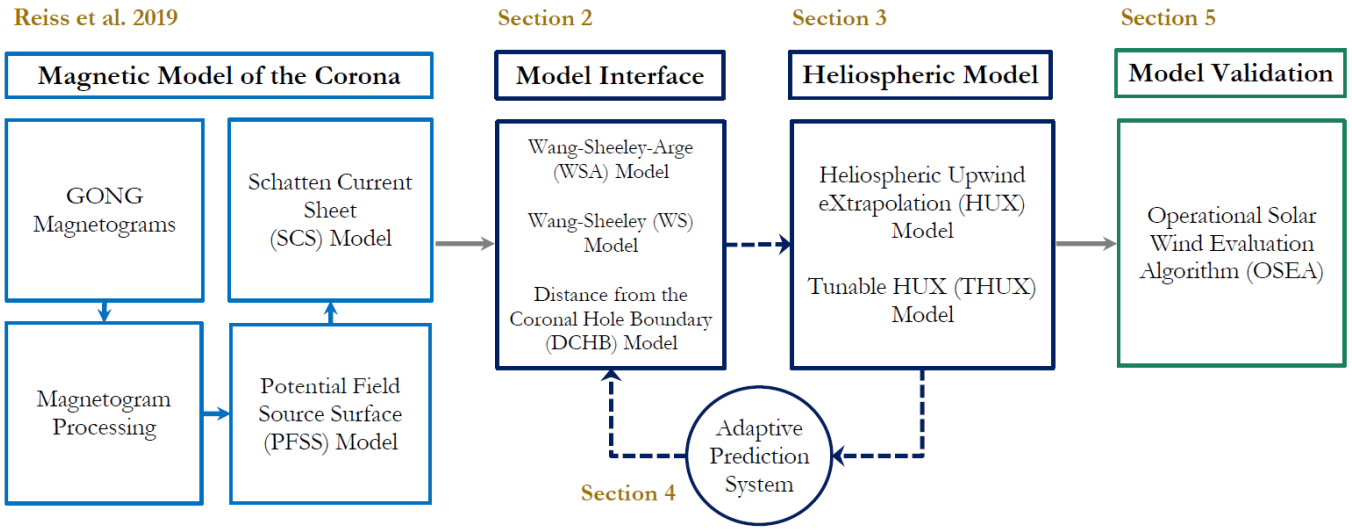

Figure 1. Overview of the approaches used in this study illustrating the adaptive system for specifying the solar wind conditions near the Sun. The sections explaining the corresponding components are indicated.

Figure 1 lays out the basic steps of the proposed strategy in detail. We use the numerical framework for modelling the ambient solar wind as recently discussed in Reiss et al. (2019). Specifically, we study different empirical techniques (WS, DCHB, and WSA model) for specifying the large-scale properties of solar wind conditions at the inner boundary of the heliospheric model. To deduce the optimum model coefficient settings, we propose an adaptive prediction system to couple **models of the ambient solar wind with** computationally efficient heliospheric propagation tools such as the Heliospheric Upwind eXtrapolation (HUX; Riley and Lionello 2011) model and the newly developed Tunable HUX model. **By doing so,** we study an ensemble of possible solar wind solutions, quantitatively estimate the model uncertainties and deduce confidence boundaries. This paper is **divided into the following** main sections. In Section 2, we **outline the components** of the numerical framework as described in Reiss et al. (2019). In Section 3, we present the proposed modifications to the HUX model for **propagating solar wind streams** from the Sun to the vicinity of Earth. In Section 4, we present the adaptive prediction system for specifying solar wind conditions near the Sun. In Section 5, we show a detailed validation analysis of our solar wind solutions for the period 2006–2015 using the Operational Solar Wind Evaluation Algorithm (OSEA; Reiss et al. 2016); and in Section 6, we conclude with a summary of the results, discuss their implications, and outline how the proposed strategies can be used effectively in operational prediction systems.

2. MODELING APPROACH

This section is concerned with summarizing the main components of the numerical framework for operating, validating, and optimizing models of the evolving ambient solar wind as discussed in greater depth in Reiss et al. (2019) and references therein. We use magnetic maps of the photospheric magnetic field from the Global Oscillation Network Group (GONG) from the National Solar Observatory (NSO) as an inner boundary condition to derive the global coronal magnetic field **(see, Figure 1)**. The magnetic maps measured in Gauss (G) are given on the $\sin(\theta)$-ϕ grid with 180×360 grid points, where $\theta \in [0, \pi]$ and $\phi \in [0, 2\pi]$ are the latitude and

longitude coordinates, respectively. They are available as near real-time magnetic maps or full **CR maps** at the GONG online platform.[1]

The magnetic model of the corona couples the PFSS model **and the Schatten current sheet (SCS) model** to reconstruct the global topology of the solar magnetic field. The PFSS model (PFSS; Altschuler and Newkirk 1969; Schatten et al. 1969) attempts to find the potential coronal field with an outer boundary condition that the magnetic field is radial ($B_\theta = B_\phi = 0$) at a reference sphere, commonly known as source surface, at $R_1 = 2.5\,R_0$. By forcing the magnetic field to become radial at the source surface, we simulate the effect of the solar wind flow in dragging out magnetic field lines. **Furthermore, we use the SCS model (Schatten 1971) in the region $R_1 \leq r \leq 2\,R_1$ to account for the latitudinal invariance of the radial magnetic field component** as observed by *Ulysses* interplanetary field measurements (Wang and Sheeley 1995).

Due to the presence of discontinuities in the form of kinks in the field line configuration at the model interface, the coupling of the PFSS and SCS model is not straightforward. McGregor et al. (2008) addressed this difficulty and proposed a more flexible coupling of the models by setting the radius of the source surface to $2.5\,R_0$ and using the PFSS solution at $2.3\,R_0$ as an inner boundary condition for the SCS model. We follow this recommendation to **couple the PFSS and SCS model to derive the global magnetic field configuration of the solar corona.**

From the topology of the solar magnetic field, we compute the solar wind conditions near the Sun that determine the inner boundary condition for solar wind models of the heliosphere. These inner boundary conditions depend crucially on the error in the solar wind speed solution. Empirical formulae for specifying the solar wind speed near the Sun rely on magnetic features computed from the configuration of open magnetic field lines. The areal expansion factor

$$f_\mathrm{p} = \left(\frac{R_0}{R_1}\right)^2 \left|\frac{\mathbf{B}(R_0,\theta_0,\phi_0)}{\mathbf{B}(R_1,\theta_1,\phi_1)}\right|, \tag{1}$$

describes the amount by which a flux tube expands between the photosphere and some reference height in the corona (Wang and Sheeley 1990). In contrast, the great-circle angular distance d refers to the distance between open field footpoints and the nearest coronal hole boundary. It is based on the idea that the solar wind is slow near coronal hole boundaries and fast inside regions of open magnetic field topology (Riley et al. 2001).

The most popular techniques for specifying the solar wind speed $v(d, f_\mathrm{p})$ at a reference sphere of $5\,R_0$ (or $30\,R_0$ for the MAS model) are the WS model (Wang and Sheeley 1990), the DCHB model (Riley et al. 2001), and the WSA model (Arge et al. 2003). The WS relation is based on the inverse relationship between the solar wind speed and the magnetic field expansion factor (Wang and Sheeley 1990), namely

$$v_\mathrm{ws}(f_\mathrm{p}) = a_1 + \frac{(a_2 - a_1)}{f_\mathrm{p}^{\,a_3}}. \tag{2}$$

[1] https://gong2.nso.edu/archive/patch.pl?menutype=s

There is evidence that low magnetic field expansion between the photosphere and some reference height in the corona is correlated with a fast solar wind speed, and vice versa (e.g., Levine et al. 1977). For the coefficients in Equation 2, we use $a_1 = 240$, $a_2 = 800$, and $a_3 = 0.34$, respectively.

The DCHB model correlates the speed at the photosphere with the distance of an open magnetic field footpoint from the nearest coronal hole boundary and maps the calculated solar wind speed solution along the field lines to a given reference sphere (Riley et al. 2001). The DCHB relation is of the form

$$v_{\rm dchb}(d) = b_1 + \frac{1}{2}\left(b_2 - b_1\right)\left[1 + \tanh\left(\frac{d - b_3}{b_4}\right)\right], \tag{3}$$

where b_3 is a measure for the thickness of the slow flow band, and b_4 denotes the width over which the solar wind reaches coronal hole values. For an open field footpoint located at the coronal hole boundary, the solar wind speed is equal to b_1. For a footpoint located deep inside a coronal hole, the solar wind speed is equal to b_2. This means that the farther away the footpoint is from the coronal hole boundary the faster the expected solar wind speed. In this study, we use $b_1 = 250$, $b_2 = 750$, $b_3 = 0.14$, and $b_4 = 0.07$ as **the default model parameter settings**.

Finally, the WSA model is a combination of the WS model and the DCHB model that unifies the expansion factor computed from the topology of the magnetic field and the distance from the coronal hole boundary (Arge et al. 2003). The WSA relation for specifying solar wind speed near the Sun is given by

$$v_{\rm wsa}(f_{\rm p}, d) = c_1 + \frac{c_2}{(1 + f_{\rm p})^{c_3}}\left\{c_4 - c_5\ \exp\left[-\left(\frac{d}{c_6}\right)^{c_7}\right]\right\}^{c_8}, \tag{4}$$

where c_i are model coefficients. For the coefficients in Equation 4 we use the following settings, $c_1 = 250$, $c_2 = 650$, $c_3 = 0.29$, $c_4 = 1$, $c_5 = 0.8$, $c_6 = 3$, $c_7 = 1.75$ and $c_8 = 3$. **Finally, we use these empirical techniques as input for models of the heliosphere that propagate the large-scale solar wind solutions from $5\,R_0$ to 1 au.** For a more detailed description of the present numerical framework for modeling the evolving ambient solar wind, we would like to refer the reader to Reiss et al. (2019) and references cited therein.

3. THE TUNABLE HELIOSPHERIC UPWIND EXTRAPOLATION (THUX) MODEL

Several heliospheric models have been proposed to map the solar wind solutions near the Sun to Earth using the coronal model solutions as a boundary condition, each with their own strengths and limitations. The broad spectrum of numerical techniques includes ballistic approximations where each parcel of plasma is assumed to travel with a constant speed through the interplanetary space, to more sophisticated global heliospheric MHD models which attempt to cover all relevant dynamical processes (e.g., Riley et al. 2011; Odstrcil 2003). In an attempt to optimize the tradeoff between accuracy and processor requirements, Riley and Lionello (2011) developed the Heliospheric Upwind eXtrapolation (HUX) model by simplifying the fluid momentum equation as much as possible. The authors proposed to neglect the pressure gradient and the gravitation term in the fluid momentum equation to obtain the inviscid form of **the one-dimensional Burgers equation** defined as

$$-\Omega_{\rm rot}\frac{\partial v_r}{\partial \phi} + v_r\frac{\partial v_r}{\partial r} = 0, \tag{5}$$

where v_r is the radial solar wind speed, ϕ is the Carrington longitude, and $\Omega_{\rm rot}$ is the rotation period of the Sun. Using a forward difference scheme in radial and longitudinal direction, the above equation can be rewritten as

$$-\Omega_{\rm rot}\left(\frac{v_{k+1}^n - v_k^n}{\Delta\phi}\right) + v_k^n\left(\frac{v_k^{n+1} - v_k^n}{\Delta r}\right) = 0, \tag{6}$$

where the indices n and k denote the radial and longitudinal grid cells, respectively. As outlined in Riley and Lionello (2011), we can rewrite the above equation to obtain

$$v_k^{n+1} = v_k^n + \frac{\Delta r\,\Omega_{\rm rot}}{v_k^n}\left(\frac{v_{k+1}^n - v_k^n}{\Delta\phi}\right). \tag{7}$$

When reaching the transition of the coronal/heliospheric model domain, the solar wind plasma has been significantly accelerated towards its final asymptotic speed. However, in the inner heliosphere beyond the coronal model domain, a residual acceleration of the plasma is expected (Schwenn 1990). To account for this effect, we follow the approach as discussed in Riley and Lionello (2011) and simulate the expected residual acceleration by an acceleration term written as

$$v_{acc} = \alpha\; v_{sw}\left(1 - \exp\left[-\frac{r}{r_H}\right]\right), \tag{8}$$

where v_{sw} is the computed solar wind bulk speed at the outer boundary of the coronal domain as discussed in Section 2, α is a model coefficient which determines the expected acceleration, and r_H is a scale length over which the acceleration is expected (Riley and Lionello 2011). **Finally,** the solar wind speed as a function of the distance $v(r)$ is given by

$$v(r) = v_{sw} + v_{acc}. \tag{9}$$

The established HUX model approach has the advantage that it can match the dynamical evolution explored by global heliospheric MHD codes while having only low computational requirements (Owens et al. 2017). **This implies that the model is ideally suited for an application in the field of data assimilation to optimally combine the model output with solar wind observations (see, Lang and Owens 2019).** However, previous research comparing observations and ambient solar wind model predictions have found that the complex evolution of wind flows in the interplanetary space results in uncertainties in the predicted arrival times of high-speed streams of more than 24 hours (see, for instance, Reiss et al. 2016). **For this reason, we propose a modification of the original HUX model which we call Tunable HUX (THUX) model. The THUX model solves the viscous form of the underlying Burgers equation.** By adding an additional term on the right-hand side of Equation 6, we obtain the viscid form of the Burgers equation given by

$$-\Omega_{\rm rot}\frac{\partial v_r}{\partial\phi} + v_r\frac{\partial v_r}{\partial r} = \eta\frac{\partial^2 v_r}{\partial\phi^2}, \tag{10}$$

where the right-hand side represents the resistance to deformation in propagating the solar wind solutions from the Sun to Earth. Using a central difference scheme for the second derivative on the right-hand side, we can write Equation 10 on a discretized grid as

$$-\Omega_{\rm rot}\left(\frac{v_{k+1}^n - v_k^n}{\Delta\phi}\right) + v_k^n\left(\frac{v_k^{n+1} - v_k^n}{\Delta r}\right) - \eta\left(\frac{u_{k+1}^n - 2\,u_k^n + u_{k-1}^n}{\Delta\phi^2}\right) = 0. \tag{11}$$

Transforming the above equation then yields an expression for the solution of the THUX model written as

$$v_k^{n+1} = v_k^n + \frac{\Omega_{\rm rot}\,\Delta r}{v_k^n}\left(\frac{v_{k+1}^n - v_k^n}{\Delta\phi}\right) + \frac{\eta\,\Delta r}{v_k^n}\left(\frac{u_{k+1}^n - 2\,u_k^n + u_{k-1}^n}{\Delta\phi^2}\right), \tag{12}$$

where η is a model coefficient that controls the resistance to deformation in the solar wind solution. In Figure 2, we illustrate the process of mapping the solar wind solutions near the Sun to the vicinity of Earth using the coupled WSA/HUX and WSA/THUX model. Figure 2(a) shows the solar wind speed solution computed at 5 R_0 and mapped along the magnetic field lines to the photosphere, as well as the photospheric footpoints connected to the sub-Earth points at the inner boundary of the heliospheric model at 5 R_0. To match the spatial resolution with the resolution of the coronal model, we use $\Delta\phi = 2^\circ$ and $\Delta r = 1\,R_0$, respectively. Figure 2(b) shows the initial solar wind solutions at the sub-Earth points (dashed black line) and the solar wind solutions for different η values at $215\,R_0$ (or 1 au). **Figure 2(c) compares the predicted solar wind speed timelines at Earth using the WSA/HUX model and the WSA/THUX model for two different η values with in situ measurements of the ambient solar wind at Earth by the Solar Wind Electron Proton and Alpha Monitor (SWEPAM; McComas et al. 1998) onboard the Advanced Composition Explorer (ACE; Stone et al. 1998) for CR2052. While maintaining the benefits of the HUX model including the low processor requirements (see, for instance, Riley and Lionello 2011; Owens et al. 2017), the THUX gives us the possibility to better account for the changing conditions in the ambient solar wind throughout the solar activity cycle. In particular, it is well suited to examine a large number of initial conditions and to deduce error bounds in the context of an adaptive prediction system for specifying solar wind conditions near the Sun.**

4. AN ADAPTIVE PREDICTION SYSTEM FOR SPECIFYING SOLAR WIND SPEED

We present an adaptive prediction system to align the large-scale properties of solar wind speed at the inner boundary of the heliospheric model with the prevailing physical conditions in the vicinity of Earth. The description of the adaptive prediction system is divided into three steps. **In Section 4.1, we present a sensitivity analysis of the WSA model for specifying solar wind speed near the Sun. We identify the model coefficients that have the lowest impact on the model output and deduce the ranking of the coefficients. By removing these coefficients from the adaptive prediction scheme, we reduce the computational complexity and processor requirements as much as possible. We note that this step is particularly important for the application of the proposed methodology in the context of real-time operational solar wind predictions. In Section 4.2, we study robust and efficient strategies for creating**

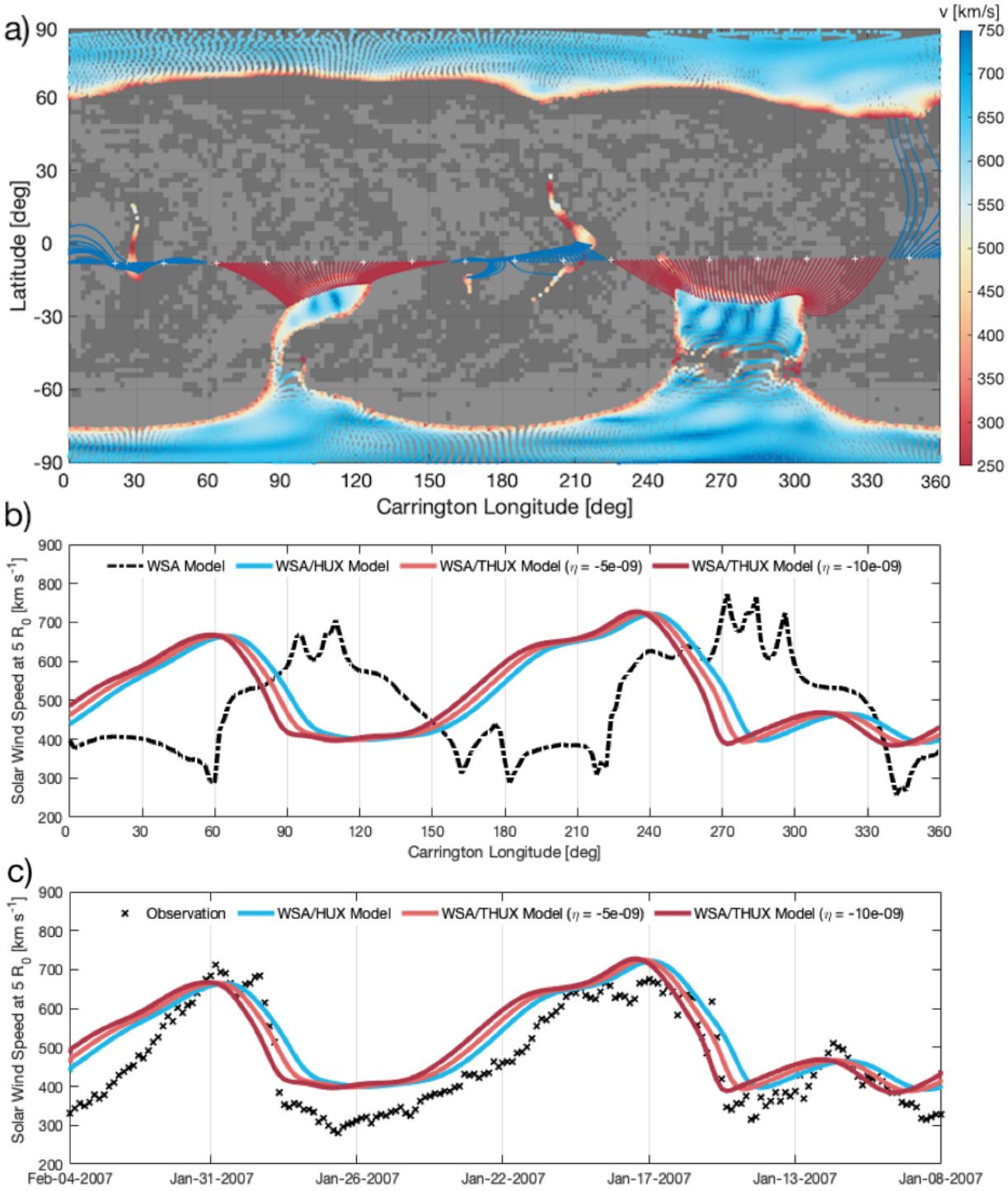

Figure 2. Illustration of the coupled WSA/THUX model for predicting the solar wind speed at Earth on the example of CR2052 (i.e., 2007 January 08–2007 February 4). (a) Solar wind speed computed at 5 R_0 using the WSA model and mapped along the magnetic field lines to 1 R_0. The grey-coloured pixels indicate closed field lines with negative (dark grey) and positive (light grey) magnetic polarity. The field lines show the photospheric footpoints connected to the sub-Earth points at the inner boundary of the heliospheric model at 5 R_0. (b) Solar wind speed computed at 5 R_0 and propagated to Earth/L1 using the HUX model and the THUX model for two different η values; (c) Comparison of the ACE/SWEPAM measurements (black crosses) and the predicted solar wind speed at Earth/L1.

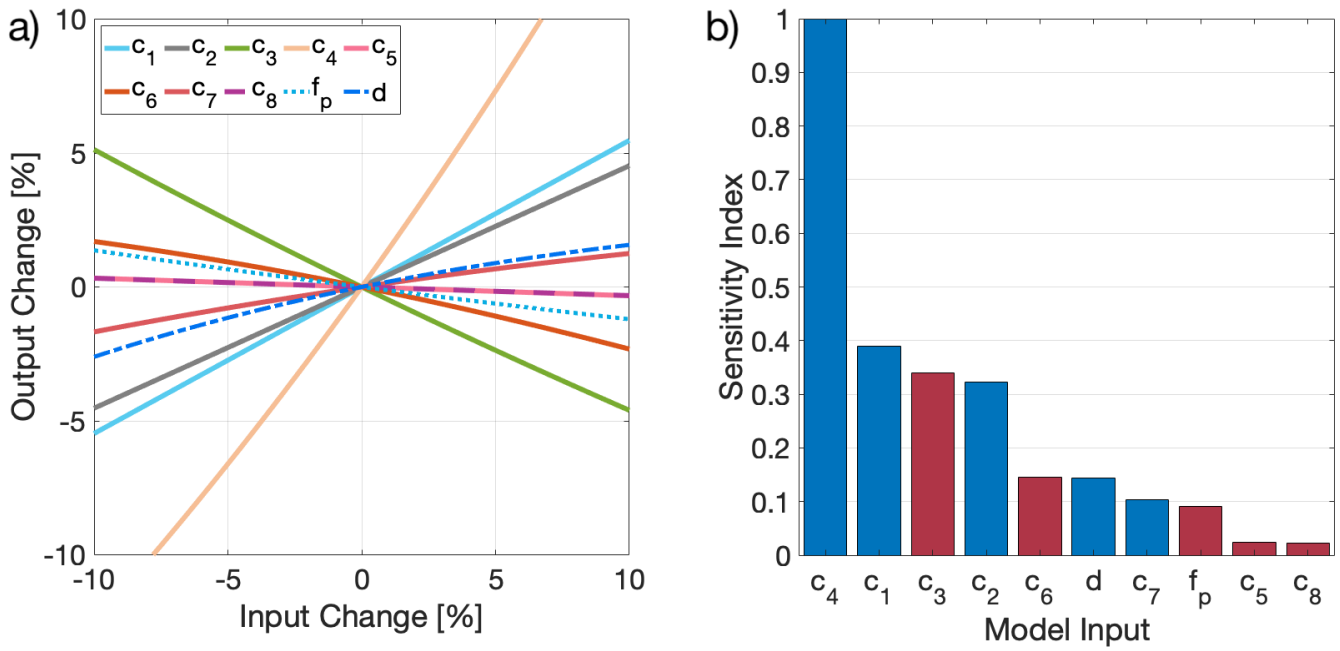

Figure 3. Sensitivity analysis of the analytic WSA relation as defined in Equation 4 for specifying solar wind speed near the Sun. (a) Output samples against input samples of different input factors for the WSA model relation with a step size of 0.1 percent; (b) Value of sensitivity index $S_i(\bar{x})$ for different input factors. The blue and red coloured bars indicate positive and negative correlations, respectively.

an ensemble of solar wind solutions; and in Section 4.3, we select the optimum model coefficients for the adaptive prediction system and deduce confidence boundaries of the solar wind prediction.

4.1. *Sensitivity analysis*

Sensitivity analysis quantitatively assesses how the variation in the output of numerical models can be attributed to variations of the model input (Pianosi et al. 2016). **The last two decades have seen a growing trend towards sensitivity analysis in the space weather forecasting and modelling community for assessing the robustness of the model results to uncertain inputs and model assumptions. More recently, model developers have shown an increased interest in using sensitivity analysis to study ensembles of solar wind predictions from perturbed initial conditions** (see, for instance, Riley et al. 2013; Owens et al. 2017; Linker et al. 2017). Although ensemble forecasting has become a very popular technique in the context of solar wind prediction, little attention has been paid to uncertainties in the model settings. In this section, we study the sensitivity **of the WSA model** on perturbed model settings. For the sake of clarity and consistency, we refer to the areal expansion factor f_p and the distance from the coronal hole boundary d in the described solar wind models as *model parameters* and refer to the model coefficients $(c_1, \ldots, c_8)$ as *input factors*.

We apply sensitivity analysis to generate a ranking of the input factors and to identify the input factors that have little impact on the WSA model output. Since the functional relation of the WSA model is available in analytic form in Equation 4, we can apply

the simplest type of sensitivity analysis by varying the input factors from their nominal settings one at a time. The solar wind speed computed from the WSA model is given by $y = v_{\mathrm{wsa}}(\mathbf{c}) = v_{\mathrm{wsa}}(c_1, \ldots, c_8)$, where $\mathbf{c}$ is the input vector and c_i are the individual input factors. We compute the output sensitivity to the i-th input factor by the partial derivative $\partial y/\partial c_i$ at the nominal value of the input factors $\bar{c}$. Hence, the sensitivity measure for the i–th input factor c_i is defined as

$$S_i(\bar{c}) = p_i \frac{\partial y}{\partial c_i}\bigg|_{\bar{c}}, \tag{13}$$

where p_i is a scaling factor. A more in-depth analysis of this type is to measure the global sensitivity by calculating output perturbations from multiple points $\mathbf{c}^j$ within the input space. A well known approach in this context is the so called Elementary Effect Test (EET) where the mean of r finite differences (also called Elementary Effects) is taken as a measure of global sensitivity given by

$$\hat{S}_i = \frac{1}{r}\sum_{j=1}^{r} |S_i(\bar{c})| = \frac{1}{r}\sum_{j=1}^{r} \left| c_i \frac{\partial y}{\partial c_i} \right|. \tag{14}$$

Intuitively one would expect that high values of $\hat{S}_i$ indicate that the input factor is more relevant to the global sensitivity of the model than other input factors. Figure 3(a) shows the output samples against samples of different input factors. Figure 3(b) shows the results of the EET for the WSA model for specifying solar wind speed at the inner boundary of the heliospheric model domain. We find that the WSA relation as given in Equation 4 is most sensitive to the input factors c_4, c_1, c_3, and c_2 (listed in decreasing order) while the influence of the other input factors is considerably smaller. Therefore, we will rely on the adjustment of the mentioned model input factors to create an ensemble of solar wind solutions at the inner boundary of the heliospheric model. By doing so, we minimize the processor requirements of the adaptive prediction system for the WSA model without neglecting decisive information content.

4.2. *Producing a solar wind speed ensemble*

A key scientific goal in the space weather research community is to develop, implement and optimize numerical models for specifying the large-scale properties of solar wind conditions at the inner boundary of the heliospheric model domain. The numerical models usually rely on empirical formulae for computing solar wind speed. However, the input factors in the literature can vary dramatically depending on the model implementation and input data products (see, e.g., Arge et al. 2003; MacNeice 2009b; Nikolic et al. 2014; Riley et al. 2015; Pomoell and Poedts 2018). **Here we propose a study of an ensemble of possible solar wind solutions** around the default model input factors to quantitatively estimate the model uncertainties and deduce confidence boundaries. Our sampling strategy to create an ensemble of solutions is built on r points in the input space, where the starting point is defined by the default input factors as discussed Section 2. **We obtain the subsequent points in the input space by modifying one input factor at a time by a fixed amount of $\delta = 2$ percent, where we define the set of**

incremental percentage adjustments to the input factors used to create the ensemble as L. Consequently, the number of ensemble members is the number of elements of L to the power of the total number of input factors. As an example, using the set of incremental percentage adjustments $L = [-4, -2, 0, 2, 4]$ for the input factors c_1, c_2, c_3, and c_4, we create an ensemble of solar wind solutions including $5^4 = 625$ ensemble members.

To propagate each ensemble member from 5 R_0 to 215 R_0 (1 au), we use the THUX model with seven different values for $\eta = [-15e^{-9}, -10e^{-9}, -5e^{-9}, 0, 5e^{-9}, -10e^{-9}, 15e^{-9}]$. We note that modifying η by steps of $5e^{-9}$ changes the arrival time of detected high-speed enhancements (HSE; Reiss et al. 2016) in the solar wind timelines by approximately 7.5 hours. Using seven different values for η implies that the number of individual solar wind solutions at Earth is $625 \times 7 = 4375$. Since the computational requirements increase exponentially with the number of input factors, the screening of input factors in Section 4.1 is an essential part of the proposed adaptive prediction system for the WSA model. Furthermore, we note that the value range and step size for L and η were determined by balancing the tradeoff between computer requirements and predictive capabilities while considering only physics-based solar wind solutions at the inner boundary of the heliospheric model part.

4.3. *Selecting the optimum input factors and deducing confidence boundaries*

Validation metrics play a central role in space weather research and forecasting to objectively assess the model agreement with measurements, to constantly diagnose and inform model developers about strength and limitations of the model, and to provide a consistent assessment of the model progress over time. Ideally, ambient solar wind models should be able to accurately simulate both the amplitude and pattern of variability in the solar wind timeline. In reality, the importance of the model skill in terms of a point-to-point error analysis or event-based analysis depends on the application, and it is therefore not possible to define a single metric that can express all relevant aspects. **In this section, we will discuss the application of two validation metrics, with one focusing on the amplitude and one on the pattern of variability.** We note that the selected validation metric in the adaptive system can easily be replaced by another metric depending on the user needs.

Each member of the ensemble discussed in Section4.2 can be associated with a summary scalar variable, for example, a measure of the difference between the measurement m_i and each ensemble member f_i. As such, the **euclidean distance (ED)** can be written as

$$\mathrm{ED} = \sqrt{\sum_{i=1}^{n} (m_i - f_i)^2}. \tag{15}$$

The best $N = 1000$ solutions from the previous CR are used to update the model coefficients for the present CR. Similar to the approach in Riley et al. (2017), all ensemble members are ranked based on the computed Euclidean distance. The top $N = 1000$ solar wind solutions are used to update the model input factors for the next CR. In this way, we constantly adapt the model coefficients, compute the ensemble median and deduce confidence boundaries for the prediction. We note that

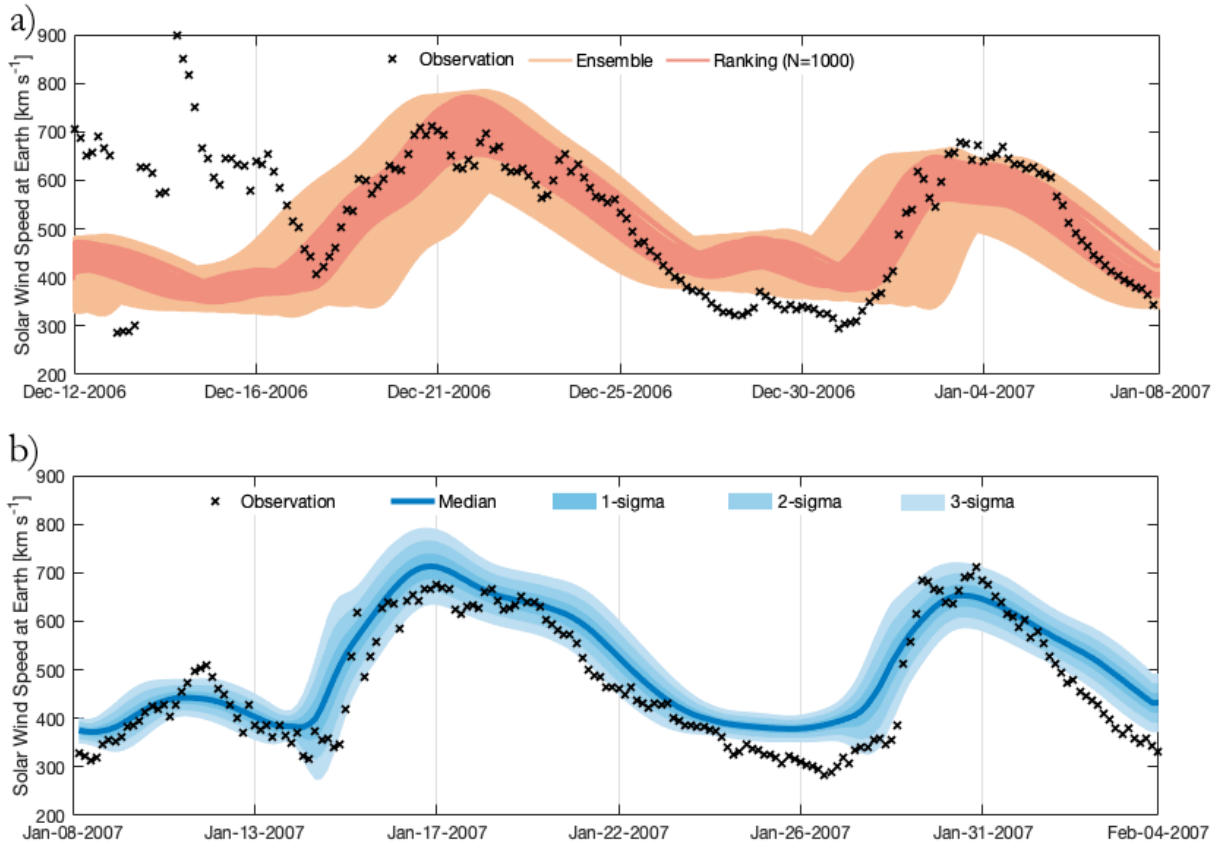

Figure 4. Illustration of the adaptive model system on the example of Carrington Rotation 2051–2052 (i.e., 2006 December 12–2007 February 4). (b) Process of training an ensemble of solutions (light-red) to better match the solar wind conditions in the vicinity of Earth (black crosses). The best $N = 1000$ solutions (red) are then used to update the model coefficients for the current Carrington Rotation. (a) Comparison of the solar wind speed measurements (black crosses), and the median of the best solutions as deduced from the previous Carrington Rotation (blue line) together with the 1-sigma, 2-sigma, and 3-sigma quantiles.

the ensemble median is the preferred average measure as the ensembles of solar wind solutions are often skewed, such that the ensemble mean can yield very biased measures of the ensemble average.

Additionally, we study a validation metric focusing on the pattern of variability (see, Taylor 2001). Given the model variables f and the measurement as a reference r, the score S_0 is defined as

$$S_0 = \frac{4(1+C)}{(\hat{\sigma}_f + 1/\hat{\sigma}_f)^2(1+C_0)}, \tag{16}$$

where $\hat{\sigma}_f$ is the ratio of the standard deviations of the model and the observation ($\hat{\sigma}_f = \sigma_f/\sigma_r$), and C_0 is the maximum correlation coefficient that can be expected. For estimating the maximum correlation coefficient we followed the approach discussed in Taylor (2001). It is clear when $\hat{\sigma}_f$ is equal to 1, that is, when the standard deviation of the model and observation are equal, and C is equal to C_0 the score S_0 goes to 1.

Figure 4 illustrates the application of the adaptive prediction system on the example of CR2052. Figure 4(a) shows the training process of CR2052 based on CR2051. The shaded areas indicate the ensemble members as outlined in Section 4.2, and the red lines indicate the selected solutions based on the computed Euclidean distance. Figure 4(b) shows the median of the ensemble members and the computed error boundaries from the 1000 best model solutions. It is important to note that ensemble averaging of possible future states does not necessarily provide an improvement of deterministic predictions (Jolliffe and Stephenson 2003; Wilks 2011). The key advantage of ensemble modelling is the quantitative assessment of prediction uncertainty including error boundaries (e.g., Owens et al. 2017).

5. ASSESSING MODEL QUALITY

We present a validation analysis of solar wind predictions with in situ measurements of the ambient solar wind at Earth/L1 by ACE/SWEPAM (Stone et al. 1998; McComas et al. 1998) for the time 2006 December 12 – 2015 September 7. We quantitatively assess the skill of the proposed prediction system by the Operational Solar Wind Evaluation Algorithm (OSEA; Reiss et al. 2016; Reiss et al. 2019). OSEA is an open-source Matlab algorithm that runs various predication validation schemes to quantitatively assess the skill of numerical models for predicting the evolving ambient solar wind in the near-Earth environment.

Traditionally, the relationship between forecast and observation can be studied in terms of continuous variables and binary variables. While the former can take on any real values, the latter is restricted to two possible values such as event/non-event. In the context of solar wind prediction, the solar wind speed time series can be interpreted in terms of both aspects. The forecasting performance can either be evaluated in terms of an **average error or its capability in forecasting events** of enhanced solar wind speed (see, for instance, Owens et al. 2005; MacNeice 2009a,b; Reiss et al. 2016). **OSEA is capable of quantifying both aspects, i.e., a continuous variable validation** based on simple point-to-point comparison metrics, and an event-based validation analysis assessing the uncertainty of arrival time of high-speed solar wind streams at Earth.

This section is organized into three parts. First, we present the validation results in terms of established error functions. Secondly, we discuss the forecast performance in terms of binary metrics where each time step in the predicted and observed timeline is labelled as an event/non-event based on the selected threshold value. We summarize the predictive capabilities of the numerical models for a range of event thresholds by the receiver operator characteristic (ROC) curve. Thirdly, we complement our validation analysis by an event-based approach where periods of enhanced solar wind speed, hereinafter referred to as high-speed enhancements (HSE), in predictions and measurements are automatically detected and compared against.

5.1. *Error functions*

The skill of model predictions of solar wind speed is commonly assessed by error functions such as the root mean square error (see, for example, Wilks 2011). To complement error functions of this type, we use the *skill score* (SS) of a prediction expressed as

$$\mathrm{SS} = 1 - \frac{\mathrm{MSE}_{\mathrm{pred}}}{\mathrm{MSE}_{\mathrm{ref}}}, \tag{17}$$

Table 1. The statistical properties of solar wind predictions for CR2047–2167 in terms of arithmetic mean (AM), standard deviation (SD), mean error (ME), mean absolute error (MAE), root mean square error (RMSE), the skill score (SS) relative to the climatological mean, and the Pearson correlation coefficient (PCC). The 27-day persistence model is a baseline reference model against which the prediction models can be compared.

Model	AM [$\mathrm{km\,s^{-1}}$]	SD [$\mathrm{km\,s^{-1}}$]	ME [$\mathrm{km\,s^{-1}}$]	MAE [$\mathrm{km\,s^{-1}}$]	RMSE [$\mathrm{km\,s^{-1}}$]	SS	PCC
WSA	469.9	82.9	-56.7	91.1	111.0	**-0.34**	0.43
Adaptive-WSA(ED)	449.5	71.9	-36.2	75.4	93.6	**0.05**	0.50
Adaptive-WSA(S_0)	480.0	85.4	-66.7	91.7	111.8	**-0.36**	0.51
WS	**414.3**	**66.4**	**0.1**	**77.0**	**99.4**	**-0.27**	**0.29**
Adaptive-WS(ED)	**414.4**	**62.2**	**0.1**	**69.4**	**90.1**	**-0.06**	**0.41**
Adaptive-WS(S_0)	**419.5**	**65.7**	**-4.5**	**71.6**	**92.6**	**-0.25**	**0.39**
DCHB	432.5	79.7	-19.2	81.1	103.3	**-0.16**	0.34
Adaptive-DCHB(ED)	428.0	75.3	-14.7	71.9	92.7	**0.06**	0.45
Adaptive-DCHB(S_0)	434.9	75.8	-21.6	74.7	95.3	**0.01**	0.43
Persistence (27-days)	415.1	96.5	-0.5	92.7	121.6	-0.59	0.20
Observation	414.5	95.7	-	-	-	-	-

where $\mathrm{MSE_{pred}}$ is the mean square error of the predicted timeline, and $\mathrm{MSE_{ref}}$ is the MSE of a reference baseline model. **We use the climatological mean defined as the mean value of the solar wind observation (413.3 $\mathrm{km\,s^{-1}}$) as a reference baseline model (see, for instance, Owens 2018).** The SS quantifies the improvement over a naive prediction model. Ideally, the prediction skill results in a zero MSE and hence in a SS value of 1. A prediction which equals the skill of the baseline model results in a SS value of 0, and a prediction which is less skilful than the baseline model results in a negative SS value.

Table 1 shows the results obtained from the continuous variable validation of different solar wind models for CR2047 to CR2167 in terms of the arithmetic mean (AM), standard deviation (SD), mean error (ME), mean absolute error (MAE), root mean square error (RMSE), and the skill score relative to the climatological mean (SS). While not strictly an error function, we complement our statistical analysis by the **Pearson correlation coefficient (PCC)**. We study the adaptive approach for ambient solar wind models (WSA, WS, and DCHB model), and run the adaptive system based on the discussed metrics ED and S_0 in Section 4.3. A 27-day **persistence model of solar wind speed is a reference baseline model for all the metrics computed in this study against which the predictive capabilities can be compared.**

We find that the RMSE for the WSA, WS, and DCHB model is 111.0 $\mathrm{km\,s^{-1}}$, 99.4 $\mathrm{km\,s^{-1}}$, and 103.3 $\mathrm{km\,s^{-1}}$, respectively. **The fluctuations in the predicted solar wind speeds for the WS model are relatively low (SD = 66.4 $\mathrm{km\,s^{-1}}$). This implies that the WS model benefits greatly in terms of the RMSE for predicting less variability and not for predicting the arrival of enhanced solar wind speeds.** The results indicate that the adaptive prediction system

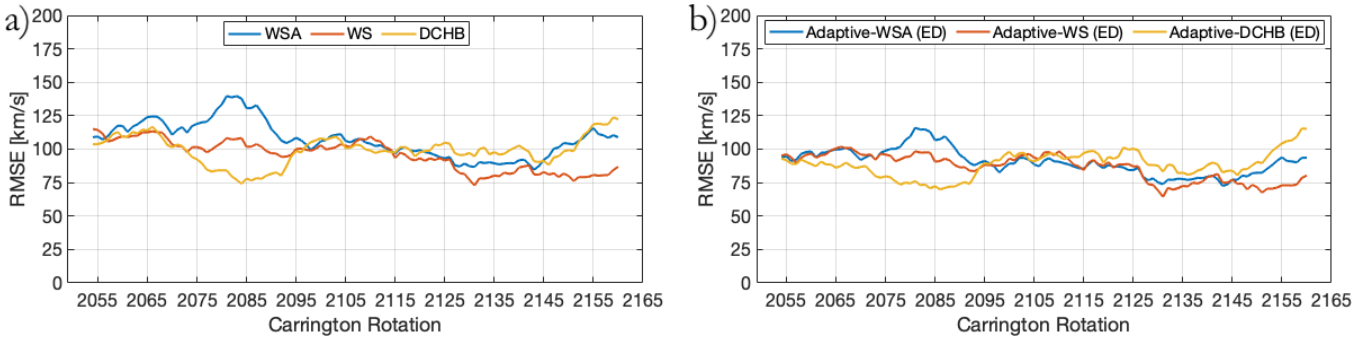

Figure 5. Comparison of an 11-Carrington rotation running average of the root mean square error (RMSE) for the WSA (blue), WS (red), and the DCHB model (yellow). (a) Results before the application of the adaptive prediction scheme; (b) Results after the application of the adaptive prediction scheme.

using the ED metric improves the capabilities of all three model approaches in terms of the described error functions. For example, the RMSE for the adaptive WSA, WS, and DCHB model using the ED metric is 93.6 km s^{-1}, 90.1 km s^{-1}, and 92.7 km s^{-1} which corresponds to a relative improvement of about 10–15 percent. The same tendency is observable for the correlation coefficient with a relative improvement of about 15–30 percent. Although the **PCC** also increases by about 15–30 percent, we find that the results for the S_0 metric are less promising and provide no improvement **for the WSA model in terms of simple point-to-point comparison metrics**.

Figure 5 shows a comparison of an 11-rotation running average of the RMSE for the WSA, WS, and the DCHB with and without the application of the adaptive prediction scheme. The results indicate that the adaptive prediction scheme generally reduces the RMSE even when the solar activity starts to increase during the year 2010. We also find that the period January 2009–October 2009 (i.e., CR2079–CR2089) is problematic for both the WS model and the WSA model. In comparison, the DCHB model tends to produce better predictions of the solar wind conditions during this interval. We suspect that the presence of unipolar streamers (also known as pseudo-streamers) is artificially raising the baseline of the predicted speed. In context, pseudo-streamers are an important diagnostic for models of the ambient solar wind because they are associated with slow to intermediate speeds despite having very low expansion factors (e.g., Riley and Luhmann 2011). In general, this characteristic is in contradiction to the basic idea of the WS and the WSA model and the DCHB model thus outperforms these models during the presence of pseudo-streamers.

It should also be noted that all the models produce better results than the reference baseline model (i.e., SS ≥ -0.59 and RMSE ≤ 121.6). The 27-day **persistence** has the same statistics as the measurements and benefits from the quasi-steady and persistent nature of the ambient solar wind flow, especially during the solar minimum phase when polar coronal holes cover a large part of the solar surface. Since our analysis includes times of low and high solar activity, the 27-day persistence model is in reasonable agreement with the observations (e.g., RMSE = 121.6 km s^{-1}). **Overall, these results indicate** that the adaptive model approach using the ED metric improves all the investigated ambient solar wind models, and performs better than the reference baseline model in terms of the computed error functions.

Table 2. Contingency table entries and skill measures of solar wind speed events during CR2047–2167 defined by an event threshold of $v > 450\text{km}\,\text{s}^{-1}$. The table shows the number of Hits (true positives; TPs), False Alarms (false positives; FPs), Misses (false negatives, FNs), Correct Rejections (true negatives, TNs), observed (P) and forecast events (P_F), and observed (O) and forecast (O_F) non-events. The last three entries in each row show the Threat Score (TS), True Skill Statistics (TSS), and Bias (BS).

Model	TP	FP	FN	TN	TPR	FPR	TS	TSS	BS
WSA	4265	6786	1665	8227	0.72	0.45	0.34	0.27	1.86
Adaptive-WSA(ED)	4094	4961	1836	10052	0.69	0.33	0.38	0.36	1.53
Adaptive-WSA(S_0)	4684	7159	1246	7854	0.79	0.48	0.36	0.31	1.99
WS	**2503**	**3197**	**3427**	**11816**	**0.42**	**0.21**	**0.27**	**0.21**	**0.96**
Adaptive-WS(ED)	**2774**	**2627**	**3156**	**12386**	**0.47**	**0.17**	**0.32**	**0.29**	**0.91**
Adaptive-WS(S_0)	**2896**	**3048**	**3034**	**11965**	**0.49**	**0.20**	**0.32**	**0.29**	**1.00**
DCHB	2909	4343	3021	10670	0.49	0.29	0.28	0.20	1.22
Adaptive-DCHB(ED)	3121	3268	2809	11745	0.53	0.22	0.34	0.31	1.08
Adaptive-DCHB(S_0)	3325	3959	2605	11054	0.56	0.26	0.34	0.30	1.23
Persistence (27-days)	2165	3708	3728	11279	0.37	0.25	0.23	0.12	1.00

5.2. *Binary metrics*

While error functions measure the magnitude of the prediction error at every time step, an alternative approach is to consider each time step as an event/non-event. As discussed in Owens (2018), this approach has some advantages over simple point-to-point error measures. First, error functions give equal importance to periods of slow solar wind and periods of fast solar wind, but some users might be interested in the accurate prediction of fast solar wind stream while the detailed evolution of the slow solar wind is of secondary importance. Secondly, outliers in the solar wind time series can have a significant impact on error functions and correlation coefficients. Thus for end-users wanting to react when the solar wind state exceeds a certain threshold, an efficient approach is to consider each time step in the solar wind solution as an event/non-event state.

In this study, we use an event threshold of $v_{\text{sw}} > 450\ \text{km}\,\text{s}^{-1}$ to define events and non-events in the solar wind timelines. By cross-checking events/non-events in the predicted and observed wind timelines we count the number of hits (*true positives*; TPs), false alarms (*false positives*; FPs), misses (*false negatives*, FNs) and correct rejections (*true negatives*, TNs). From the number of instances, summarized in the so-called contingency table, we compute different skill measures such as the *true positive rate* $\text{TPR} = \text{TP}/(\text{TP} + \text{FN})$, *false positive rate* $\text{FPR} = \text{FP}/(\text{FP} + \text{TN})$, *threat score* $\text{TS} = \text{TP}/(\text{TP}+\text{FP}+\text{FN})$, *bias* $\text{B} = (\text{TP}+\text{FP})/(\text{TP}+\text{FN})$, and *true skill statistics* $\text{TSS} = \text{TPR}-\text{FPR}$. The TSS is defined in the range $[-1, 1]$ where a perfect prediction model would have the value 1 (or -1 for a perfect inverse event prediction), and a TSS of 0 indicates no skill. The TSS has the advantage that it uses all elements in the contingency table, and is unbiased by the proportion of predicted and observed events (Hanssen and Kuipers 1965; Bloomfield et al. 2012). For further reading on this type of validation measures, we would like to refer the interested reader to Owens (2018).

Table 3. Statistics of the detected high-speed enhancements in terms of event-based metrics including the number of observed (P) and forecast (P_F) events, the Bias (BS), the number of Hits (TPs), False Alarms (FPs), and Misses (FNs) together with the Probability of Detection (POD), False Negative Rate (FNR), Positive Predictive Value (PPV), False Alarm Ratio (FAR), and Threat Score (TS).

Model	P	P_F	BS	TP	FP	FN	POD	FNR	PPV	FAR	TS
WSA	301	286	0.92	161	125	140	**0.53**	**0.47**	**0.56**	**0.44**	**0.38**
Adaptive-WSA(ED)	301	213	0.68	143	70	158	**0.47**	**0.53**	**0.67**	**0.33**	**0.39**
Adaptive-WSA(S_0)	301	246	0.78	159	87	142	**0.53**	**0.47**	**0.65**	**0.35**	**0.41**
WS	301	**193**	**0.64**	**122**	**71**	**179**	**0.41**	**0.59**	**0.63**	**0.37**	**0.33**
Adaptive-WS(ED)	301	**167**	**0.55**	**121**	**46**	**180**	**0.40**	**0.60**	**0.72**	**0.28**	**0.35**
Adaptive-WS(S_0)	301	**170**	**0.56**	**119**	**51**	**182**	**0.40**	**0.60**	**0.70**	**0.30**	**0.34**
DCHB	301	279	0.92	148	131	153	0.49	0.51	0.53	0.47	0.34
Adaptive-DCHB(ED)	301	206	0.68	136	70	165	0.45	0.55	0.66	0.34	0.37
Adaptive-DCHB(S_0)	301	235	0.78	146	89	155	0.49	0.51	0.62	0.38	0.37
Persistence (27-days)	313	314	1.0	142	172	171	0.45	0.55	0.45	0.55	0.29

Table 2 shows the contingency table entries and skill measures of solar wind speed events during CR2047–2167 defined by an event threshold of $v = 450$ km s^{-1}. The TSS for the WS, DCHB, and WSA model is **0.21, 0.20, and 0.27** respectively. We find that the TSS for the adaptive prediction system systematically increases. **Specifically, the TSS for the newly proposed adaptive WS, DCHB, and WSA model using the ED metric (S_0 metric) is 0.29 (0.29), 0.31 (0.30), and 0.36 (0.31), respectively**.

The combination of the proportion of correctly predicted events (TPR) and the proportion of falsely predicted events (FPR) in the TSS complement each other and provide deep insight into the capabilities of the model prediction. A way to summarize the predictive capabilities for a range of different event thresholds is the so-called receiver operator characteristic (ROC) curve. **The ROC curves illustrate how the number of correctly predicted events (TPR) varies with the number of incorrectly predicted non-events (FPR). Figure 6(a)–(c)** shows the resulting ROC curves for the WSA model, WS model, and DCHB model together with the climatological mean. We find that for all the model combinations the results are above the $y = x$ line in **Figure 6** indicating that TPR > FPR for all the ambient solar wind models. A comparison of the different ROC curves shows that the adaptive prediction system improves the results for all the event thresholds. **We quantitatively assess this improvement by the computed area under the curve (AUC). The AUC is a summary variable defined between 0 and 1 and an indication of how well the models can predict the ambient solar wind. The analysis shows that the AUC increases for all the adaptive models by approximately 5 percent.**

In parallel to that analysis, we use the Taylor diagram to summarize different validation metrics in a single diagram (Taylor 2001). In recent years, the Taylor diagram has become a popular means to present multiple aspects of model validation in a single diagram (e.g., Riley et al. 2013; Owens 2018). The key of constructing such a diagram is to recognize the geometric relationship between

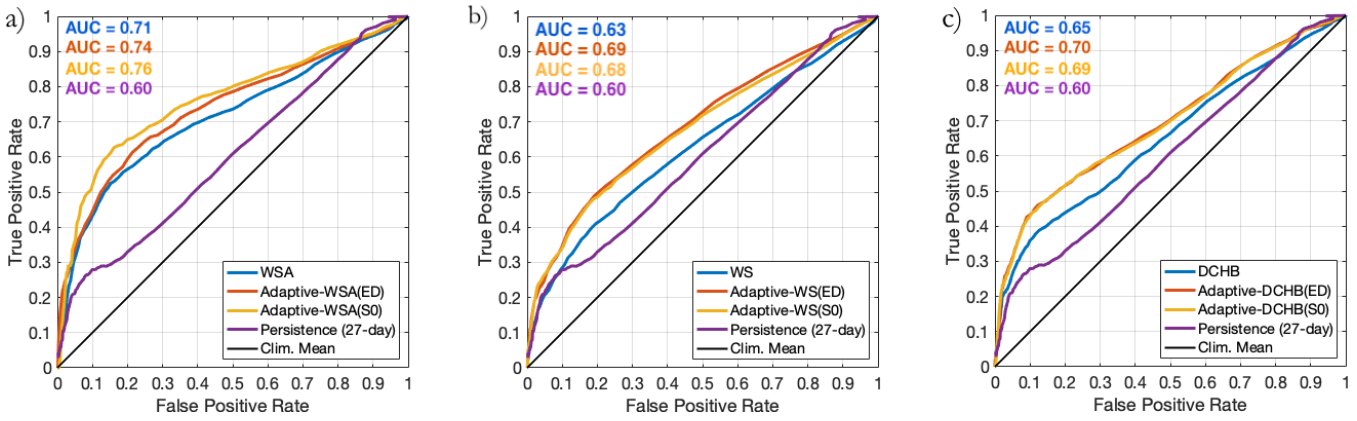

Figure 6. Receiver operator characteristic curves plotting the true positive rate (TPR) against the false positive rate (TPR) for a range of event thresholds for different models of the ambient solar wind including the WSA model, WS model, and the DCHB model (a)–(c), together with the 27-day persistence model (violet line) and the climatological mean (black line). The area under the curve (AUC) on the left hand corner is a summary variable of how well the model can predict the ambient solar wind.

the correlation coefficient, the RMSE, and the amplitude of variations in the predicted and reference time series (see, Taylor 2001). In this way, we compare different model results and trace the impact of the proposed modifications. As shown in **Figure 7**, the azimuthal position indicates the **PCC**, the radial distance from the circle at the x-axis is proportional to the RMSE, and the distance from the origin is proportional to the amplitude of variations (standard deviation). Thus, model predictions in perfect agreement with the observations will be located very close to the circle on the x-axis indicated by similar standard deviation, high correlation and low RMSE. The distance from the circle on the x-axis refers to the overall model performance in terms of the underlying validation metrics. To complement the results displayed in the Taylor diagram, we use a colourmap indicating the TSS value from the discussed event/non-event analysis (see, Table 2). **Figure 7** shows that all the solar wind solutions using the adaptive prediction system are located closer to the observation. The arrows in **Figure 7** highlight the improvement of the WSA, WS, and DCHB model by the application of the adaptive model approach.

5.3. *Event-based metrics*

A core difficulty facing any validation analysis that uses error functions as quantitative validation measures is an inadequate knowledge of the uncertainties due to timing errors (see, Owens 2018). The interpretation of simple point-to-point error measures can be misleading as discussed in the scientific literature (see, for example, Owens et al. 2005; MacNeice 2009a,b). A validation analysis is very challenging, for example, when the evolution of significant leaps in the timelines are generally well predicted, but the arrival times differ slightly in prediction and observation. To account for the uncertainty in the arrival times, we use an event-based validation approach as discussed in greater depth in Reiss et al. (2016). More specifically, the validation analysis applied in this section consists of three steps. First, we define and detect events of enhanced solar wind speed, also called high-speed enhancements (HSEs) in forecast and observation

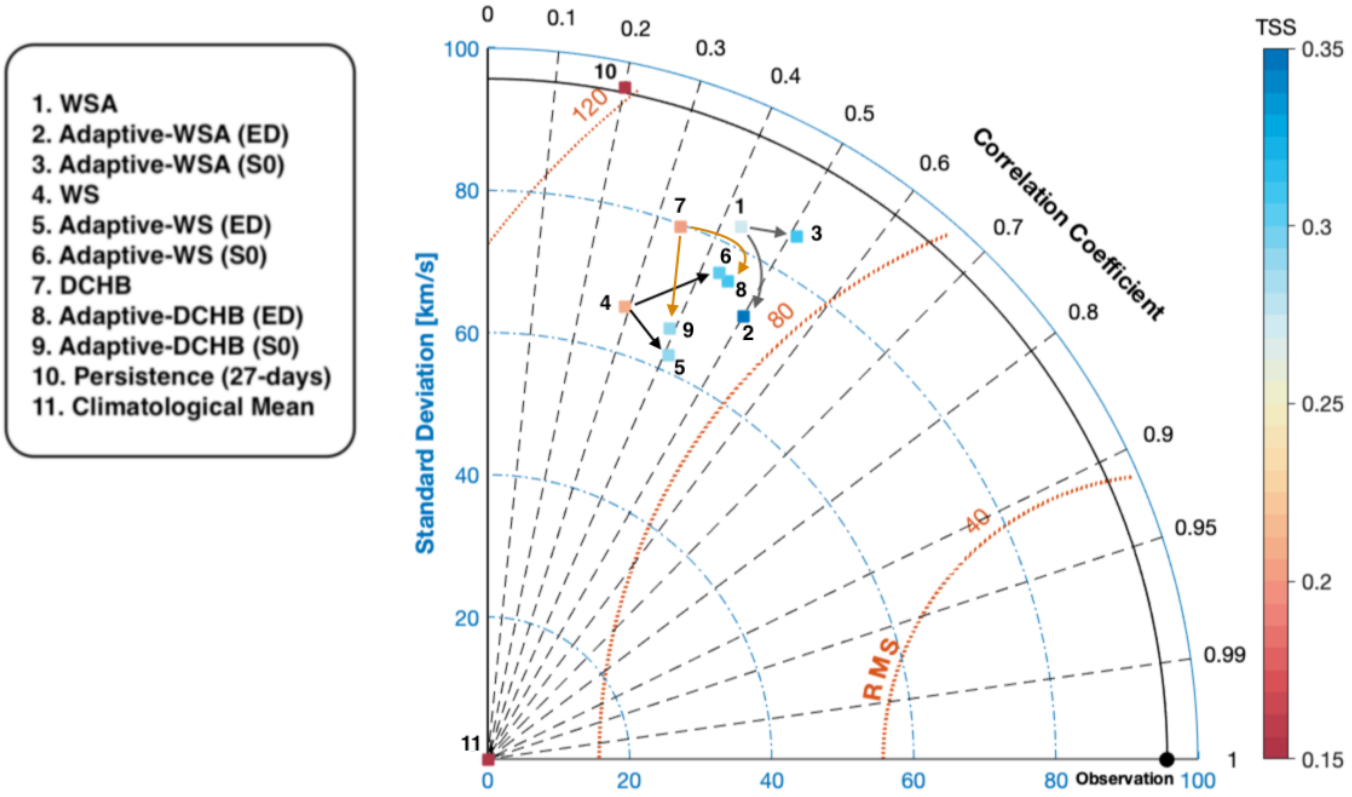

Figure 7. Taylor Diagram for displaying a summary of different validation metrics, including the standard deviation, root mean square error (RMSE) and Pearson correlation coefficient (PCC). The diagram compares the predictive capabilities of the WSA model, WS model, DCHB model, Adaptive-WSA model, Adaptive-WS model, Adaptive-DCHB model, persistence model, and the climatological mean with the measured solar wind speed for CR2047–CR2167. The colourmap complements the computed error functions by displaying the TSS calculated from an event/non-event based validation analysis as outlined in Section 5.2.

data. Secondly, we associate the HSEs detected in the solar wind measurements with HSEs detected in the prediction and label each event pair as a hit, false alarm, or miss. Thirdly, we compute different validation summary variables to present and compare the predictive abilities of the investigated models.

Table 3 shows the number of observed (P) and forecast (P_F) events, the Bias (BS), the number of Hits (TPs), False Alarms (FPs), and Misses (FNs) together with the Probability of Detection (POD), False Negative Rate (FNR), Positive Predictive Value (PPV), False Alarm Ratio (FAR), and Threat Score (TS). With a minimum event speed limit of 450 km s^{-1}, the POD for the WSA is 0.53, the FNR is 0.47, the PPV is 0.56, and the FAR is 0.44. This means that about 53 percent of the observed HSEs are correctly predicted by the WSA model, and 47 percent of all predicted HSEs are observed. In contrast, the POD for the Adaptive-WSA model is 0.53, the FNR is 0.47, the PPV is 0.65, and the FAR is 0.35. This indicates that the adaptive prediction system reduces the number of false alarms by about 30 percent. A similar improvement is observable for the other models, with the false alarms for the WS and DCHB being reduced by 25 and 30 percent, respectively. In comparison, the TS for the WSA model is 0.38 whereas the TS for the Adaptive-WSA(ED) is 0.39.

Although times of recorded ICMEs according to the list [2] of Richardson and Cane (Richardson and Cane 2010) are excluded from our analysis, all ambient solar wind models have in common that they systematically underestimate the number of observed HSEs (BS $\leq$ 0.92). To support a consistent and transparent assessment of space weather modeling products, we have uploaded all the discussed validation measures and the updated validation functions to the OSEA online repository[3].

6. DISCUSSION

In this study, we presented an adaptive prediction system that fuses information from in situ observations of the evolving ambient solar wind flow into numerical models to better match the global solar wind solutions near the Sun with prevailing physical conditions in Earth's space weather environment. A novel element of our procedure is the replacement of static empirical formulae by a more flexible approach for specifying solar wind conditions near the Sun. We coupled the continuously updated solar wind conditions with computationally efficient heliospheric propagation tools such as the HUX model and the newly developed THUX model to deduce the optimum model coefficient settings for the following Carrington rotation. By doing so, we studied an ensemble of possible solar wind solutions, quantitatively estimated the model uncertainties and deduced confidence boundaries. Finally, we applied a comprehensive validation analysis based on simple point-to-point error measures and event-based measures, and compare our results to reference benchmark models. Our study leads us to two primary conclusions:

i) solving the viscous form of the Burgers equation in the newly proposed THUX model provides a robust and efficient method to study, adapt, and optimize the input variability space of established empirical relationships between the magnetic field topology and the near-Sun solar wind conditions including the WS, DCHB and WSA model; and

ii) the results show that the application of the proposed adaptive prediction system improves the abilities of models of the ambient solar wind for real-time operational purposes according to the community validation measures applied.

We find that the proposed prediction scheme improves all the investigated coronal/heliospheric model combinations and that both of our conclusions have an essential impact on enhancing the predictive abilities of the model approaches investigated. Although the basic idea of the THUX model was to provide us with an efficient means to study a variety of solar wind model solutions, we find that the application of the THUX without the adaptive process in the empirical speed formulae also improves the results. As an example, we find that in the case of the WSA model this approach reduces the RMSE to 107.8 km/s and increases the CC to 0.45. We can therefore deduce that the application of the THUX alone has a positive impact on the results, even without the application of the full adaptive prediction scheme. Furthermore, it should be noted that our results for the WSA model with the default model settings, are in reasonable agreement with other studies (e.g., Owens et al. 2008; Reiss et al. 2016). This implies that the described methodology using the default model parameter settings is starting from a similar level of forecasting skill and that application of the adaptive prediction system might be beneficial for other solar wind frameworks too. Another important finding is that the adaptive scheme also improves the results during periods of increased solar activity even when

[2] http://www.srl.caltech.edu/ACE/ASC/DATA/level3/icmetable2.htm
[3] https://bitbucket.org/reissmar/solar-wind-forecast-verification

the magnetic field configuration in the solar corona is highly structured, and the dynamical evolution of the evolving ambient solar wind is much more complicated.

It is crucial to bear in mind the possible uncertainties that affect the results and the conclusions of our study. An essential component in this context is the uncertainty of observed magnetic maps which influence the quality of solar wind solutions with empirical and more physics-based MHD models. Especially the process for constructing synoptic maps and the correction of the poorly observed polar regions likely has a considerable influence on the resulting model solutions (Riley et al. 2012). In view of this, one could question the ability of coronal models for reconstructing the global topology of open magnetic field lines. To seamlessly simulate the dynamics of the evolving ambient solar wind, we rely on the coupling of a magnetic model of the corona with the HUX and THUX model to map the solutions near the Sun to Earth. The coronal part of our numerical framework uses the PFSS model to reconstruct the global magnetic field configuration. Ideally, one would prefer more physics-based models to simulate the complex dynamics of the evolving ambient solar wind, especially at solar wind stream interaction regions, which are not included in the present approach. Nevertheless, recent research suggests that the predictive abilities of semi-empirical and full physics-based coupled corona/heliosphere models are very similar. As an example, Owens et al. (2008) studied the performance of different numerical frameworks (WSA, WSA/Enlil, and MAS/Enlil) and showed that the coupled semi-empirical approach gives the best results in point-to-point measures. To optimize the tradeoff between model accuracy and processor requirements of a full MHD code, we would recommend usage of the described methods, in particular, for the purpose of real-time solar wind predictions.

In the context of real-time operational solar wind prediction, it is essential to highlight that we used Carrington rotation magnetic maps to present the application of this prototype of an adaptive scheme. This means that the sub-Earth observations of the photospheric magnetic field are between 0 and 27 days old. Hence, the present framework for prediction does not correspond to real-time operational space weather frameworks for prediction of the solar wind state in the interplanetary medium and at Earth's space weather environment. Although an analysis of real-time applications is beyond the scope of this study, we speculate that usage of the most recent magnetic maps in combination with the adaptive prediction scheme with a daily update could also enhance the accuracy of real-time wind predictions.

We want to emphasize that we have conducted some additional experiments and investigated various model settings to optimize the results of the adaptive scheme which are not mentioned in this study. As an example, we studied the impact of the adaptive process on the large-scale solution of the solar wind models near the Sun to exclude non-physical solutions from the beginning. In this way, we were able to reject model settings that produced unrealistically low or high values of the solar wind speed at the polar regions. Moreover, we implicitly dealt with the problem of overfitting by allowing only for variations in the model coefficients up to a maximum of 4 percent. In addition, we studied different time windows for the adaptive process. Specifically, we increased the size of the training window up to 5 Carrington rotations but saw no significant improvement to the model results during this process. Along these lines, it is important to note that we do not claim that the present parameter settings should become a community standard. Since the framework implementation could rely on different full-disk magnetograms and could be very technically different, it is not guaranteed that the settings discussed here are suitable for all operational solar wind prediction pipelines. Instead, this

study presents the first prototype of such an implementation and we recommend that the parameter settings should be investigated based on the underlying numerical framework.

In closing, we note that there are further benefits to this approach, of which one is the improvement of deterministic forecasting by including a quantification of the associated uncertainty. Future work will look towards applying more sophisticated statistical methods to improve the adaptive process where possible, and will also look to extending the model through the inclusion of further physical properties beyond the solar wind speed. Furthermore, this approach shows promise in the application to coronal model parameters such as the source surface distance. Recent studies on the source surface distance suggest that the choice of the distance influences the results largely, and this varies with the solar activity (e.g., Lee et al. 2011; Arden et al. 2014; Nikolic 2019). A problem here is that of choosing the right model coefficients in Equation 2–4 for the solar wind models for the relevant source surface height. With the adaptive process method described here, we suggest that it might be possible to derive continuously updated boundary conditions near the Sun for the corresponding source surface height. Improvements to the boundary conditions of heliospheric models represent not only an improvement for space weather prediction but also for space weather research in general. Therefore we conclude that our study has important implications for future work in applied space weather research and prediction.

ACKNOWLEDGMENTS

The work utilizes data obtained by the Global Oscillation Network Group (GONG) Program, managed by the National Solar Observatory, which is operated by AURA, Inc. under a cooperative agreement with the National Science Foundation. The data were acquired by instruments operated by the Big Bear Solar Observatory, High Altitude Observatory, Learmonth Solar Observatory, Udaipur Solar Observatory, Instituto de Astrofísica de Canarias, and Cerro Tololo Interamerican Observatory. **The author thanks Leila M. Mays for helpful conversations about this work, and acknowledges NASA's Community Coordinated Modeling Center (CCMC) for financial travel support. M.A.R., C.M. and R.L.B. acknowledge the Austrian Science Fund (FWF): J4160-N27 and P31659-N27.**

REFERENCES

M. D. Altschuler and G. Newkirk. Magnetic Fields and the Structure of the Solar Corona. I: Methods of Calculating Coronal Fields. *SoPh*, 9:131–149, September 1969. https://doi.org/10.1007/BF00145734.

W. M. Arden, A. A. Norton, and X. Sun. A breathing source surface for cycles 23 and 24. *Journal of Geophysical Research: Space Physics*, 119(3):1476–1485, 2014. ISSN 2169-9402. https://doi.org/10.1002/2013JA019464.

C. N. Arge and V. J. Pizzo. Improvement in the prediction of solar wind conditions using near-real time solar magnetic field updates. *J. Geophys. Res.*, 105:10465–10480, May 2000. https://doi.org/10.1029/1999JA000262.

C. N. Arge, D. Odstrcil, V. J. Pizzo, and L. R. Mayer. Improved Method for Specifying Solar Wind Speed Near the Sun. In M. Velli, R. Bruno, F. Malara, and B. Bucci, editors, *Solar Wind Ten*, volume 679 of *American Institute of Physics Conference Series*, pages 190–193, September 2003. https://doi.org/10.1063/1.1618574.

C. N. Arge, J. G. Luhmann, D. Odstrcil, C. J. Schrijver, and Y. Li. Stream structure and coronal sources of the solar wind during the May 12th, 1997 CME. *Journal of Atmospheric and Solar-Terrestrial Physics*, 66:1295–1309, October 2004. https://doi.org/10.1016/j.jastp.2004.03.018.

D. Shaun Bloomfield, Paul A. Higgins, R. T. James McAteer, and Peter T. Gallagher. Toward Reliable Benchmarking of Solar Flare Forecasting Methods. *ApJL*, 747(2):L41, Mar 2012. https://doi.org/10.1088/2041-8205/747/2/L41.

M. D. Cash, D. A. Biesecker, V. Pizzo, C. A. de Koning, G. Millward, C. N. Arge, C. J. Henney, and D. Odstrcil. Ensemble Modeling of the 23 July 2012 Coronal Mass Ejection. *Space Weather*, 13:611–625, October 2015. https://doi.org/10.1002/2015SW001232.

A. Devos, C. Verbeeck, and E. Robbrecht. Verification of space weather forecasting at the Regional Warning Center in Belgium. *Journal of Space Weather and Space Climate*, 4(27): A29, October 2014. https://doi.org/10.1051/swsc/2014025.

R. M. Dewey, D. N. Baker, B. J. Anderson, M. Benna, C. L. Johnson, H. Korth, D. J. Gershman, G. C. Ho, W. E. McClintock, D. Odstrcil, L. C. Philpott, J. M. Raines, D. Schriver, J. A. Slavin, S. C. Solomon, R. M. Winslow, and T. H. Zurbuchen. Improving solar wind modeling at Mercury: Incorporating transient solar phenomena into the WSA-ENLIL model with the Cone extension. *Journal of Geophysical Research (Space Physics)*, 120:5667–5685, July 2015. https://doi.org/10.1002/2015JA021194.

A.W. Hanssen and W.J.A. Kuipers. *On the Relationship Between the Frequency of Rain and Various Meteorological Parameters: (with Reference to the Problem Ob Objective Forecasting)*. Koninkl. Nederlands Meterologisch Institut. Mededelingen en Verhandelingen. Staatsdrukerij, 1965. URL https://books.google.at/books?id=nTZ8OgAACAAJ.

L. K. Jian, C. T. Russell, J. G. Luhmann, P. J. MacNeice, D. Odstrcil, P. Riley, J. A. Linker, R. M. Skoug, and J. T. Steinberg. Comparison of observations at ace and ulysses with enlil model results: Stream interaction regions during carrington rotations 2016 – 2018. *Solar Physics*, 273(1):179–203, 2011. ISSN 1573-093X. https://doi.org/10.1007/s11207-011-9858-7.

I.T. Jolliffe and D.B. Stephenson. *Forecast Verification: A Practitioner's Guide in Atmospheric Science*. Wiley, 2003. ISBN 9780471497592. URL https://books.google.com/books?id=Qm2MjWVvUywC.

Matthew Lang and Mathew J. Owens. A Variational Approach to Data Assimilation in the Solar Wind. *Space Weather*, 17(1):59–83, Jan 2019. https://doi.org/10.1029/2018SW001857.

C. O. Lee, J. G. Luhmann, D. Odstrcil, P. J. MacNeice, I. Pater, P. Riley, and C. N. Arge. The solar wind at 1 au during the declining phase of solar cycle 23: Comparison of 3d numerical model results with observations. *Solar Physics*, 254(1):155–183, 2008. ISSN 1573-093X. https://doi.org/10.1007/s11207-008-9280-y.

Christina Lee, J. Luhmann, Todd Hoeksema, Xudong Sun, C. Arge, and I. Pater. Coronal field opens at lower height during the solar cycles 22 and 23 minimum periods: Imf comparison suggests the source surface should be lowered. *Solar Physics*, 269:367–388, 04 2011. https://doi.org/10.1007/s11207-010-9699-9.

R. H. Levine, M. D. Altschuler, and J. W. Harvey. Solar sources of the interplanetary magnetic field and solar wind. *J. Geophys. Res.*, 82: 1061–1065, March 1977. https://doi.org/10.1029/JA082i007p01061.

J. A. Linker, Z. Mikić, D. A. Biesecker, R. J. Forsyth, S. E. Gibson, A. J. Lazarus, A. Lecinski, P. Riley, A. Szabo, and B. J. Thompson. Magnetohydrodynamic modeling of the solar corona during Whole Sun Month. *J. Geophys. Res.*, 104:9809–9830, May 1999. https://doi.org/10.1029/1998JA900159.

J. A. Linker, R. M. Caplan, C. Downs, P. Riley, Z. Mikic, R. Lionello, C. J. Henney, C. N. Arge, Y. Liu, M. L. Derosa, A. Yeates, and M. J. Owens. The Open Flux Problem. *ApJ*, 848:70, October 2017. https://doi.org/10.3847/1538-4357/aa8a70.

J. G. Luhmann, M. L. Mays, D. Odstrcil, Y. Li, H. Bain, C. O. Lee, A. B. Galvin, R. A. Mewaldt, C. M. S. Cohen, R. A. Leske, D. Larson, and Y. Futaana. Modeling solar energetic particle events using ENLIL heliosphere simulations. *Space Weather*, 15: 934–954, July 2017. https://doi.org/10.1002/2017SW001617.

D. H. Mackay and A. R. Yeates. The Sun's Global Photospheric and Coronal Magnetic Fields: Observations and Models. *Living Reviews in Solar Physics*, 9:6, November 2012. https://doi.org/10.12942/lrsp-2012-6.

P. MacNeice. Validation of community models: Identifying events in space weather model timelines. *Space Weather*, 7:S06004, June 2009a. https://doi.org/10.1029/2009SW000463.

P. MacNeice. Validation of community models: 2. Development of a baseline using the Wang-Sheeley-Arge model. *Space Weather*, 7: S12002, December 2009b. https://doi.org/10.1002/2009SW000489.

P. MacNeice, B. Elliott, and A. Acebal. Validation of community models: 3. Tracing field lines in heliospheric models. *Space Weather*, 9:S10003, October 2011. https://doi.org/10.1029/2011SW000665.

M. L. Mays, B. J. Thompson, L. K. Jian, R. C. Colaninno, D. Odstrcil, C. Mstl, M. Temmer, N. P. Savani, G. Collinson, A. Taktakishvili, P. J. MacNeice, and Y. Zheng. Propagation of the 2014 January 7 CME and resulting geomagnetic non-event. *The Astrophysical Journal*, 812(2):145, October 2015. ISSN 0004-637X. https://doi.org/10.1088/0004-637X/812/2/145.

D. J. McComas, S. J. Bame, P. Barker, W. C. Feldman, J. L. Phillips, P. Riley, and J. W. Griffee. Solar Wind Electron Proton Alpha Monitor (SWEPAM) for the Advanced Composition Explorer. *SSRv*, 86:563–612, July 1998. https://doi.org/10.1023/A:1005040232597.

S. L. McGregor, W. J. Hughes, C. N. Arge, and M. J. Owens. Analysis of the magnetic field discontinuity at the potential field source surface and schatten current sheet interface in the wangsheeleyarge model. *Journal of Geophysical Research: Space Physics*, 113(A8), 2008. https://doi.org/10.1029/2007JA012330. URL https://agupubs.onlinelibrary.wiley.com/doi/abs/10.1029/2007JA012330.

Z. Mikić, J. A. Linker, D. D. Schnack, R. Lionello, and A. Tarditi. Magnetohydrodynamic modeling of the global solar corona. *Physics of Plasmas*, 6:2217–2224, May 1999. https://doi.org/10.1063/1.873474.

L. Nikolic. On solutions of the pfss model with gong synoptic maps for 20062018. *Space Weather*, 17(8):1293–1311, 2019. https://doi.org/10.1029/2019SW002205. URL https://agupubs.onlinelibrary.wiley.com/doi/abs/10.1029/2019SW002205.

L. Nikolic, L. Trichtchenko, and D. Boteler. A Numerical Framework for Operational Solar Wind Prediction. *Plasma Fusion Res.*, 9, 2014. https://doi.org/10.1585/pfr.9.3406099.

D. Odstrcil. Modeling 3-D solar wind structure. *Advances in Space Research*, 32:497–506, August 2003. https://doi.org/10.1016/S0273-1177(03)00332-6.

H.J. Opgenoorth, R.F. Wimmer-Schweingruber, A. Belehaki, D. Berghmans, M. Hapgood, M. Hesse, K. Kauristie, M. Lester, J. Lilensten, M. Messerotti, and M. Temmer. Assessment and recommendations for a consolidated european approach to space weather - as part of a global space weather effort. *J. Space Weather Space Clim.*, 9:A37, 2019. https://doi.org/10.1051/swsc/2019033.

M. J. Owens. Time-Window Approaches to Space-Weather Forecast Metrics: A Solar Wind Case Study. *Space Weather*, 16:1847–1861, November 2018. https://doi.org/10.1029/2018SW002059.

M. J. Owens, C. N. Arge, H. E. Spence, and A. Pembroke. An event-based approach to validating solar wind speed predictions: High-speed enhancements in the wang-sheeley-arge model. *Journal of Geophysical Research: Space Physics*, 110(A12): n/a–n/a, 2005. ISSN 2156-2202. https://doi.org/10.1029/2005JA011343. A12105.

M. J. Owens, H. E. Spence, S. McGregor, W. J. Hughes, J. M. Quinn, C. N. Arge, P. Riley, J. Linker, and D. Odstrcil. Metrics for solar wind prediction models: Comparison of empirical, hybrid, and physics-based schemes with 8 years of L1 observations. *Space Weather*, 6:S08001, August 2008. https://doi.org/10.1029/2007SW000380.

M. J. Owens, R. Challen, J. Methven, E. Henley, and D. R. Jackson. A 27 day persistence model of near-earth solar wind conditions: A long lead-time forecast and a benchmark for dynamical models. *Space Weather*, 11(5): 225–236, 2013. ISSN 1542-7390. https://doi.org/10.1002/swe.20040.

M. J. Owens, P. Riley, and T. S. Horbury. Probabilistic Solar Wind and Geomagnetic Forecasting Using an Analogue Ensemble or "Similar Day" Approach. *SoPh*, 292:69, May 2017. https://doi.org/10.1007/s11207-017-1090-7.

Francesca Pianosi, Keith Beven, Jim Freer, Jim W. Hall, Jonathan Rougier, David B. Stephenson, and Thorsten Wagener. Sensitivity analysis of environmental models: A systematic review with practical workflow. *Environmental Modelling Software*, 79:214 – 232, 2016. ISSN 1364-8152. https://doi.org/https://doi.org/10.1016/j.envsoft.2016.02.008. URL http://www.sciencedirect.com/science/article/pii/S1364815216300287.

J. Pomoell and S. Poedts. EUHFORIA: European heliospheric forecasting information asset. *Journal of Space Weather and Space Climate*, 8 (27):A35, June 2018. https://doi.org/10.1051/swsc/2018020.

M. A. Reiss, M. Temmer, A. M. Veronig, L. Nikolic, S. Vennerstrom, F. Schoengassner, and S. J. Hofmeister. Verification of high-speed solar wind stream forecasts using operational solar wind models. *Space Weather*, 14(7): 2016SW001390, July 2016. ISSN 1542-7390. https://doi.org/10.1002/2016SW001390.

M. A. Reiss, P. J. MacNeice, L. M. Mays, C. N. Arge, C. Möstl, L. Nikolic, and T. Amerstorfer. Forecasting the Ambient Solar Wind with Numerical Models. I. On the Implementation of an Operational Framework. *ApJS*, 240:35, February 2019. https://doi.org/10.3847/1538-4365/aaf8b3.

I. G. Richardson and H. V. Cane. Near-earth interplanetary coronal mass ejections during solar cycle 23 (1996 – 2009): Catalog and summary of properties. *Solar Physics*, 264(1): 189–237, 2010. ISSN 1573-093X. https://doi.org/10.1007/s11207-010-9568-6.

P. Riley and R. Lionello. Mapping Solar Wind Streams from the Sun to 1 AU: A Comparison of Techniques. *SoPh*, 270:575–592, June 2011. https://doi.org/10.1007/s11207-011-9766-x.

P. Riley and J. G. Luhmann. Interplanetary Signatures of Unipolar Streamers and the Origin of the Slow Solar Wind. *Solar Physics*, 277(2):355–373, December 2011. ISSN 0038-0938, 1573-093X. https://doi.org/10.1007/s11207-011-9909-0. URL http://link.springer.com/article/10.1007/s11207-011-9909-0.

P. Riley, J. A. Linker, and Z. Mikić. An empirically-driven global MHD model of the solar corona and inner heliosphere. *J. Geophys. Res.*, 106:15889–15902, August 2001. https://doi.org/10.1029/2000JA000121.

P. Riley, R. Lionello, J. A. Linker, Z. Mikic, J. Luhmann, and J. Wijaya. Global MHD Modeling of the Solar Corona and Inner Heliosphere for the Whole Heliosphere Interval. *SoPh*, 274:361–377, December 2011. https://doi.org/10.1007/s11207-010-9698-x.

P. Riley, J. A. Linker, and Z. Mikić. On the application of ensemble modeling techniques to improve ambient solar wind models. *Journal of Geophysical Research (Space Physics)*, 118: 600–607, February 2013. https://doi.org/10.1002/jgra.50156.

P. Riley, J. A. Linker, and C. N. Arge. On the role played by magnetic expansion factor in the prediction of solar wind speed. *Space Weather*, 13:154–169, March 2015. https://doi.org/10.1002/2014SW001144.

P. Riley, M. Ben-Nun, J. A. Linker, M. J. Owens, and T. S. Horbury. Forecasting the properties of the solar wind using simple pattern recognition. *Space Weather*, 15:526–540, March 2017. https://doi.org/10.1002/2016SW001589.

P. Riley, M. L. Mays, J. Andries, T. Amerstorfer, D. Biesecker, V. Delouille, M. Dumbović, X. Feng, E. Henley, J. A. Linker, C. Möstl, M. Nuñez, V. Pizzo, M. Temmer, W. K. Tobiska, C. Verbeke, M. J. West, and X. Zhao. Forecasting the Arrival Time of Coronal Mass Ejections: Analysis of the CCMC CME Scoreboard. *Space Weather*, 16:1245–1260, September 2018. https://doi.org/10.1029/2018SW001962.

Pete Riley, Jon A. Linker, R. Lionello, and Z. Mikic. Corotating interaction regions during the recent solar minimum: The power and limitations of global MHD modeling. *Journal of Atmospheric and Solar-Terrestrial Physics*, 83:1–10, Jul 2012. https://doi.org/10.1016/j.jastp.2011.12.013.

K. H. Schatten. Current sheet magnetic model for the solar corona. *Cosmic Electrodynamics*, 2: 232–245, 1971.

K. H. Schatten, J. M. Wilcox, and N. F. Ness. A model of interplanetary and coronal magnetic fields. *SoPh*, 6:442–455, March 1969. https://doi.org/10.1007/BF00146478.

C. J. Schrijver, M. L. De Rosa, T. R. Metcalf, Y. Liu, J. McTiernan, S. Régnier, G. Valori, M. S. Wheatland, and T. Wiegelmann. Nonlinear Force-Free Modeling of Coronal Magnetic Fields Part I: A Quantitative Comparison of Methods. *SoPh*, 235:161–190, May 2006. https://doi.org/10.1007/s11207-006-0068-7.

C. J. Schrijver et al. Understanding space weather to shield society: A global road map for 2015-2025 commissioned by COSPAR and ILWS. *Advances in Space Research*, 55: 2745–2807, June 2015. https://doi.org/10.1016/j.asr.2015.03.023.

R. Schwenn. *Large-Scale Structure of the Interplanetary Medium*, page 99. 1990.

C. Scolini, L. Rodriguez, M. Mierla, J. Pomoell, and S. Poedts. Observation-based modelling of magnetised coronal mass ejections with EUHFORIA. *A&A*, 626:A122, Jun 2019. https://doi.org/10.1051/0004-6361/201935053.

N. R. Sheeley, Jr. Origin of the Wang-Sheeley-Arge solar wind model. *History of Geo- and Space Sciences*, 8:21–28, March 2017. https://doi.org/10.5194/hgss-8-21-2017.

E. C. Stone, A. M. Frandsen, R. A. Mewaldt, E. R. Christian, D. Margolies, J. F. Ormes, and F. Snow. The Advanced Composition Explorer. *SSRv*, 86:1–22, July 1998. https://doi.org/10.1023/A:1005082526237.

A. Taktakishvili, M. Kuznetsova, P. MacNeice, M. Hesse, L. Rastätter, A. Pulkkinen, A. Chulaki, and D. Odstrcil. Validation of the coronal mass ejection predictions at the Earth orbit estimated by ENLIL heliosphere cone model. *Space Weather*, 7:S03004, March 2009. https://doi.org/10.1029/2008SW000448.

A. Taktakishvili, P. MacNeice, and D. Odstrcil. Model uncertainties in predictions of arrival of coronal mass ejections at Earth orbit. *Space Weather*, 8:S06007, June 2010. https://doi.org/10.1029/2009SW000543.

K. E. Taylor. Summarizing multiple aspects of model performance in a single diagram. *Journal of Geophysical Research: Atmospheres*, 106(D7):7183–7192, 2001. ISSN 2156-2202. https://doi.org/10.1029/2000JD900719.

G. Tóth et al. Space Weather Modeling Framework: A new tool for the space science community. *Journal of Geophysical Research (Space Physics)*, 110:A12226, December 2005. https://doi.org/10.1029/2005JA011126.

C. Verbeke, M. L. Mays, M. Temmer, S. Bingham, R. Steenburgh, M. Dumbović, M. Núñez, L. K. Jian, P. Hess, C. Wiegand, A. Taktakishvili, and J. Andries. Benchmarking CME Arrival Time and Impact: Progress on Metadata, Metrics, and Events. *Space Weather*, 17:6–26, January 2019. https://doi.org/10.1029/2018SW002046.

Y.-M. Wang and N. R. Sheeley, Jr. Solar wind speed and coronal flux-tube expansion. *ApJ*, 355:726–732, June 1990. https://doi.org/10.1086/168805.

Y.-M. Wang and N. R. Sheeley, Jr. Solar Implications of ULYSSES Interplanetary Field Measurements. *ApJL*, 447:L143, July 1995. https://doi.org/10.1086/309578.

Wijsen, N., Aran, A., Pomoell, J., and Poedts, S. Modelling three-dimensional transport of solar energetic protons in a corotating interaction region generated with euhforia. *A&A*, 622:A28, 2019. https://doi.org/10.1051/0004-6361/201833958.

D. S. Wilks. *Statistical methods in the atmospheric sciences*. Elsevier Academic Press, Amsterdam; Boston, 2011. ISBN 9780123850225 0123850223.

R. M. Winslow, N. A. Schwadron, N. Lugaz, J. Guo, C. J. Joyce, A. P. Jordan, J. K. Wilson, H. E. Spence, D. J. Lawrence, R. F. Wimmer-Schweingruber, and M. L. Mays. Opening a Window on ICME-driven GCR Modulation in the Inner Solar System. *ApJ*, 856:139, April 2018. https://doi.org/10.3847/1538-4357/aab098.

A. M. Wold, M. L. Mays, A. Taktakishvili, L. K. Jian, D. Odstrcil, and P. MacNeice. Verification of real-time WSA-ENLIL+Cone simulations of CME arrival-time at the CCMC from 2010 to 2016. *Journal of Space Weather and Space Climate*, 8(27):A17, March 2018. https://doi.org/10.1051/swsc/2018005.